Supporting Information

Surface Decoration on Self-supporting High Entropy Alloy Electrodes for Enhanced Electrochemical Water Splitting

Runtong Zhou[1], Xiao Han[1,2,], Qiao Chen[1], Luwei Peng[2], Xueyuan Qiu[1], Pan Wang[1], Chang Guo[1], Jincheng Wang[1], Zhijun Wang[1], Jianhua Hao[2,*]*

[1]*State Key Laboratory of Solidification Processing, School of Materials Science and Engineering, Northwestern Polytechnical University, Xi'an, 710072, PR China.*

[2]*Department of Applied Physics, The Hong Kong Polytechnic University, Hong Kong, PR China.*

[*]*Corresponding authors:*

E-mail: xiao.han@nwpu.edu.cn (X. Han)

jh.hao@polyu.edu.hk (J. Hao)

Experimental Details

Materials.

All chemicals are of commercial analysis grade and used without further purifications. Potassium hydroxide (KOH, 85%), hydrochloric acid (HCl, 36.0~38.0%), nickel (II) nitrate hexahydrate ($Ni(NO_3)_2 \cdot 6H_2O$, 98.5%), iron (III) nitrate nonahydrate ($Fe(NO_3)_2 \cdot 9H_2O$, 98%), aluminum nitrate nonahydrate ($Al(NO_3)_3 \cdot 9H_2O$, 99%), vanadium(III) chloride (VCl_3, 97%) and ethanol absolute (C_2H_5OH, EtOH, 99.7%) were purchased from Sinopharm Chemical Reagent Co. Ltd. Chloroplatinic acid hexahydrate ($H_2PtCl_6 \cdot 6H_2O$, 37.5%), ruthenium(III) chloride hydrate ($RuCl_3 \cdot xH_2O$, 37.5%), iridium chloride hydrate ($IrCl_3 \cdot xH_2O$, 52%) and Urea ($CO(NH_2)_2$, 99.5%) were purchased from Shanghai Aladdin Biochemical Technology Co. Ltd. Deionized water (DI-water) (18.25 MΩ cm^{-1}) was produced by a Water Purifier system.

Preparation of porous high-entropy alloys.

Master alloy ingots with a nominal composition of $Ni_{30}Co_{30}Cr_{10}Fe_{10}Al_{18}W_2$ (at%) were prepared by vacuum arc melting under a high-purity argon atmosphere. To ensure uniform distribution of metal elements, the ingots were remelted four times and then dropped into copper molds. HEA sheets with a length × width × height of 20 mm × 10 mm × 1 mm were obtained on a wire cutting machine, and the HEA sheets were cleaned with acetone, 3 M HCl acid, and anhydrous ethanol, respectively, for 15 min and dried in a vacuum oven for 30 min for further use. To obtain PHEA sheets, the above HEA sheets were immersed in HCl acid (3 M) solution and heated at 60 °C for 300 min to remove the B2 phase, and the de-alloyed HEA sheets were washed several times with deionized water and anhydrous ethanol and placed in a drying oven for further use.

Preparation of surface modified HEA-based electrodes.

A one-step hydrothermal method was used to grow a multivariate NiX-LDH (X=Al, Fe, V) phase *in situ* on the surface of PHEA. In brief, 0.6 mmol of $Ni(NO_3)_2 \cdot 6H_2O$, 0.48 mmol of $Al(NO_3)_3 \cdot 9H_2O$, ($Fe(NO_3)_2 \cdot 9H_2O$, VCl_3), and 4 mmol of urea are placed

into 30-ML of deionized water. The above PHEA tablets were immersed in the solution and transferred to a 50-ML PTFE-lined stainless steel autoclave. The autoclave was heated in an electric furnace to 120 °C for up to 12 h and then cooled to room temperature. The obtained electrode sheets were washed several times with deionized water and then dried in an oven at 60 ℃ to obtain NiX-LDH (X=Al, Fe, V). The *in situ* growth process of NiXY-LDH (Y=Pt, Ru, Ir) was similar to that of NiX-LDH (X=Al, Fe, V) except that 0.18 mmol of $H_2PtCl_6 \cdot 6H_2O$ was added to the electrode sheets, 0.18 mmol of $RuCl_3 \cdot xH_2O$, and 0.36 mmol of $IrCl_3 \cdot xH_2O$, respectively.

Material characterization.

XRD patterns were collected on a PAN analytical X'Pert PRO using a Cu source. A TESCAN MIRA3 microscope equipped with a TESCAN Essence™ EDS device was used to obtain SEM images and elemental distribution information. N_2 adsorption isotherms were determined using a microanalyzer ASAP2460. XPS was performed on a PHI 5000 Versa Probe III. The spectra were corrected using the C1s peak (284.8 eV) as a reference, samples were characterized without any electrochemical treatment. For TEM measurements, the LDH suspension obtained by the hydrothermal method was washed and dried by centrifugation, weigh 5 mg of powder dissolved in 1 mL of anhydrous ethanol, 20-30 uL of drops were taken into a copper mesh, dried, and then characterized on an FEI Talos F200S G2 after performing the FEI Talos F200S G2. The characteristic spectral lines in the range of 1000 cm^{-1} and 4000 cm^{-1} were recorded on a Nicolet iS50 FT-IR microscope, and the *in situ* electrochemical infrared spectra were also recorded on a Nicolet iS50 FT-IR microscope in the wavenumber range between 1000 cm^{-1} and 4000 cm^{-1} at a potential range of -0.1 V to -0.8 V (vs. reversible hydrogen electrode, RHE). Renishaw's in Via Raman microscope was applied to collect the Raman spectra with the laser wavelength of 532 nm, and a configuration of numerical aperture of 0.55 with 50× microscope objective was used in all Raman measurements, in addition, *in situ* Raman spectra were also measured on the device over a range from 200-3200 cm^{-1} with bias voltages from 0.2 V to 0.6 V (vs. Ag/AgCl).

The electrolyzer used to test Faraday efficiency was an interchangeable membrane H-cell type cell with a Nafion 117 membrane for separating the anode from the cathode to evaluate the Faraday efficiency of the NiAlPt-LDH@PHEA electrode, with the working area set to 0.5 cm^2. All gaseous products were detected online by GC7900, Shanghai, China. The thermal conductivity detector (TCD) in GC is used to detect hydrogen.

Electrochemical measurements.

The electrochemical catalytic performance was evaluated using a CHI 760E workstation with a standard three-electrode configuration. The HEA-based electrode was used directly as the working electrode, while the platinum wire and the Hg/HgO (1 M KOH) electrode were used as the counter electrode and reference electrode, respectively. Measurements were performed in 1 M KOH aqueous solution with 95% iR compensation. The standard hydrogen potential was converted using E (vs. RHE) = E (vs. Hg/HgO) + 0.059 pH + 0.098 V, using Hg/HgO as reference.

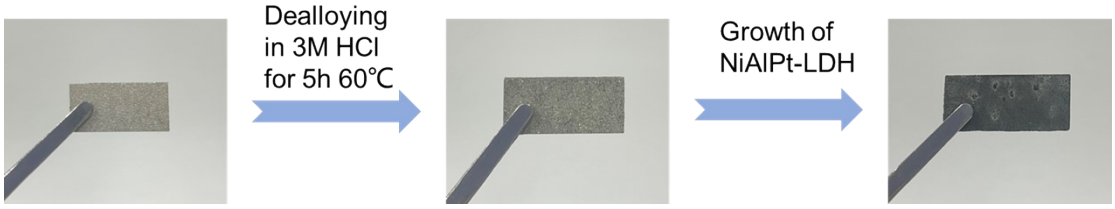

Figure S1. Digital photographs of EHEA, PHEA and NiAlPt-LDH@PHEA, respectively. As shown in the figure, the eutectic high-entropy alloy has a bright metallic luster. After acid dealloying, the color becomes darker and the thickness becomes thinner. The surface modified HEA-based electrode shows a light blue state, indicating the successful growth of LDH.

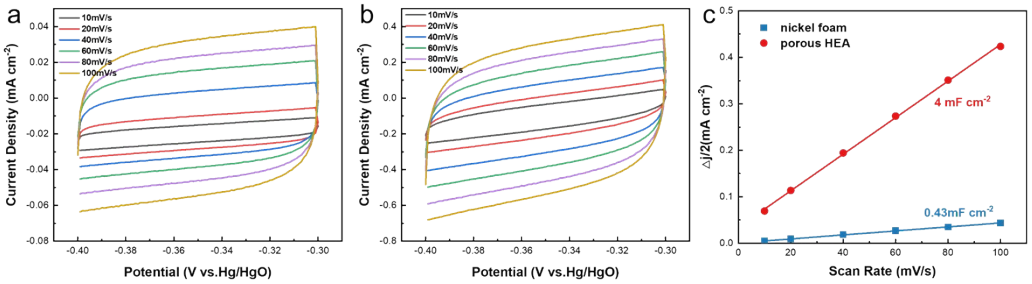

Figure S2. CV curves of various samples at different scan rate. (a) nickel foam. (b) Porous HEA. (c) C_{dl} obtained by CV cycles at given scan rate.

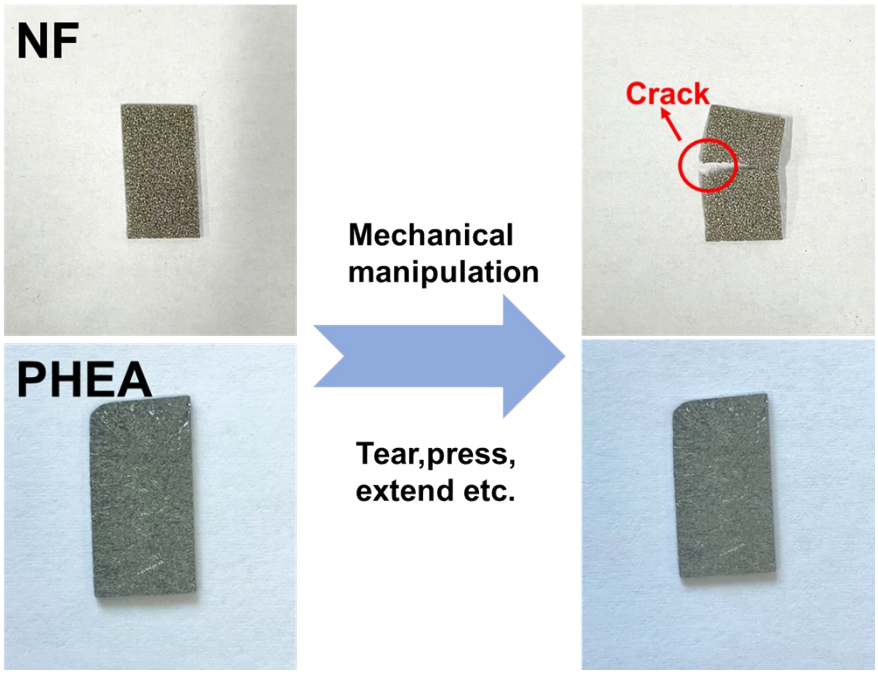

Figure S3. Digital images of NF/PHEA after multiple mechanical manipulations. NF exhibits inferior mechanical robustness and stability compared to PHEA electrode.

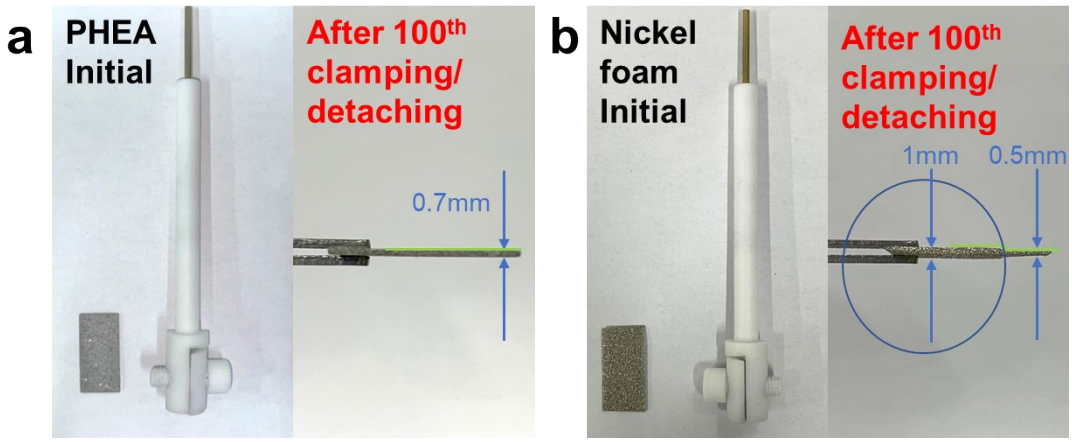

Figure S4. (a)Digital photographs of PHEA and (b) nickel foam before and after 100th clamping/detaching and their thickness variation. As shown in the figure, it is evident that after 100 electrode clamps, the thickness of the PHEA electrode hardly changes significantly, while the thickness of the NF electrode decreases significantly, which may lead to the destruction of the 3D porous structure and a decrease in specific surface area. The stacking structure may also lead to slow gas release and affect reaction activity.

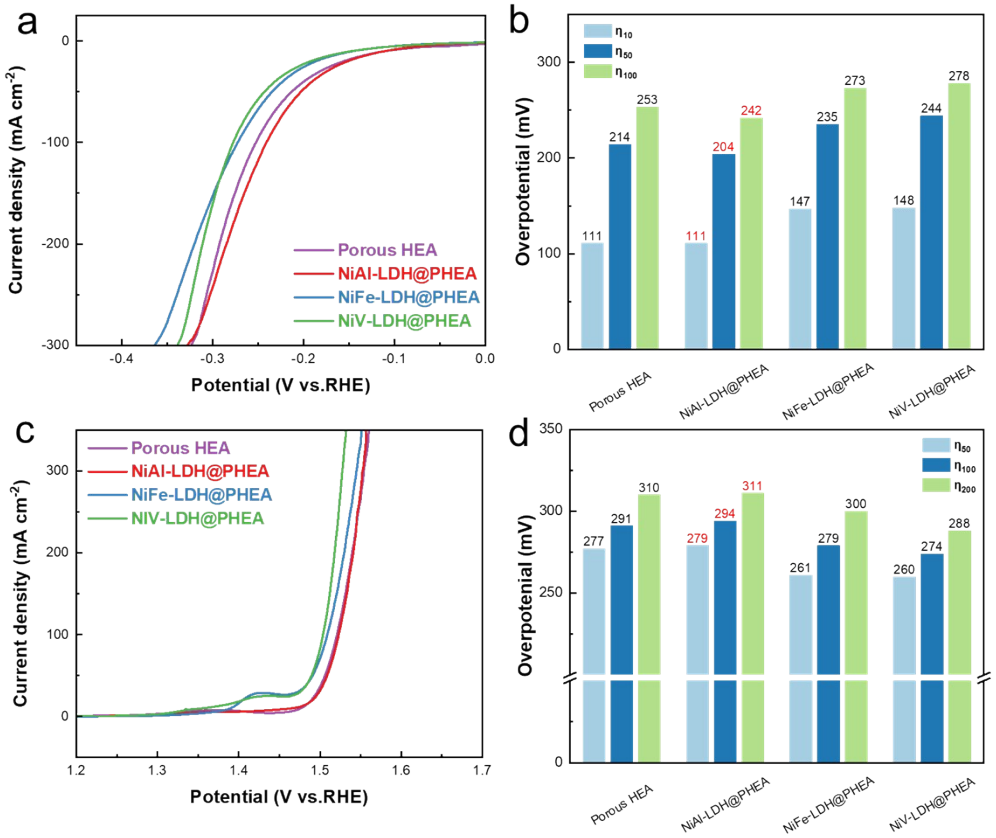

Figure S5. HER and OER performance of NiX(X=Al, Fe, V)-LDH@PHEA electrodes. (a) LSV curves for HER performance of various bulk PHEA electrodes. (b) Overpotential for HER of various bulk PHEA electrodes at different current densities (10, 50, 100 mA cm^{-2}). (c) LSV curves for OER performance of various bulk PHEA electrodes. (d) Overpotential for OER of various bulk PHEA electrodes at different current densities (50, 100, 200 mA cm^{-2}).

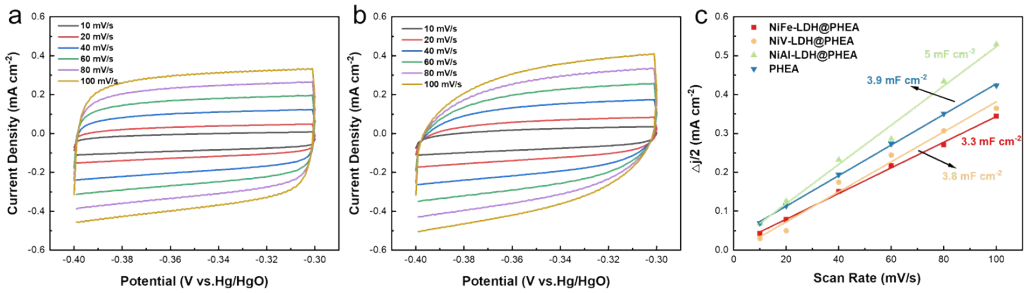

Figure S6. CV curves of various bulk electrodes at different scan rate. (a) NiFe-LDH@PHEA. (b) NiV-LDH@PHEA. (c) C_{dl} obtained by CV cycles at given scan rate.

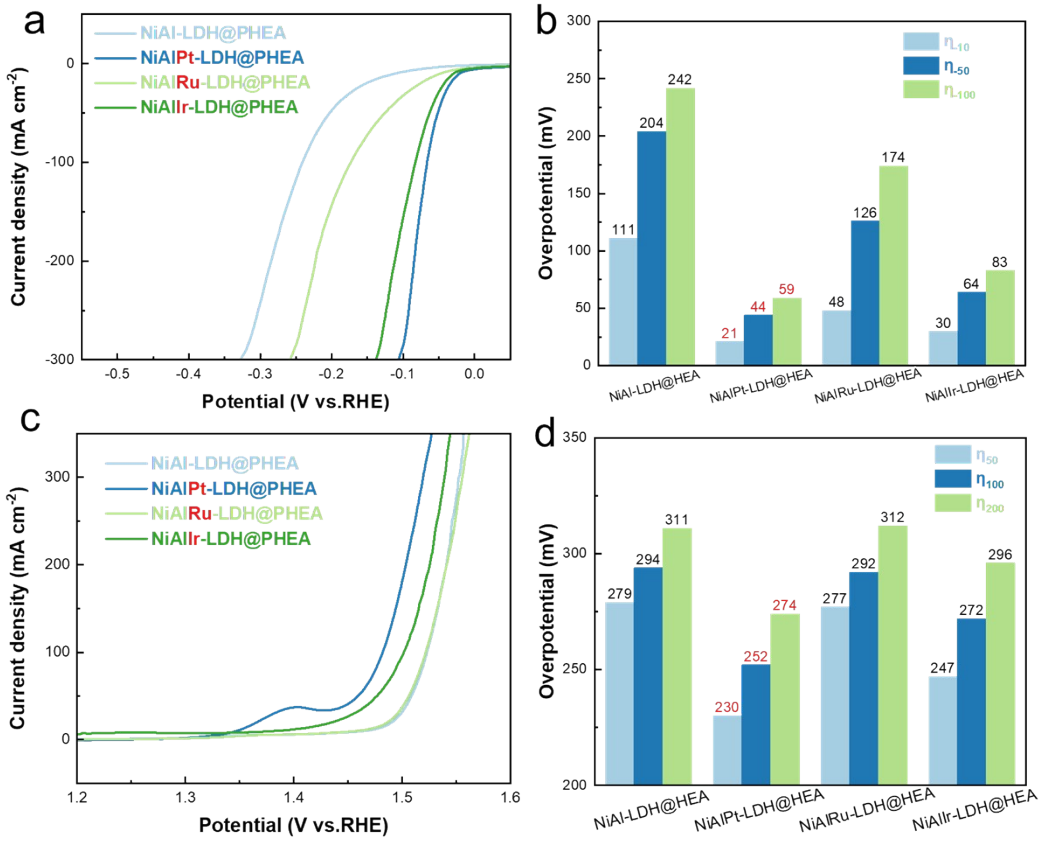

Figure S7. HER and OER performance of NiAlY(Y=Pt, Ru, Ir)-LDH@PHEA electrodes. (a) LSV curves for HER performance of various bulk PHEA electrodes. (b) Overpotential for HER of various bulk PHEA electrodes at different current densities (10, 50, 100 mA cm^{-2}). (c) LSV curves for OER performance of various bulk PHEA electrodes. (d) Overpotential for OER of various bulk PHEA electrodes at different current densities (50, 100, 200 mA cm^{-2}).

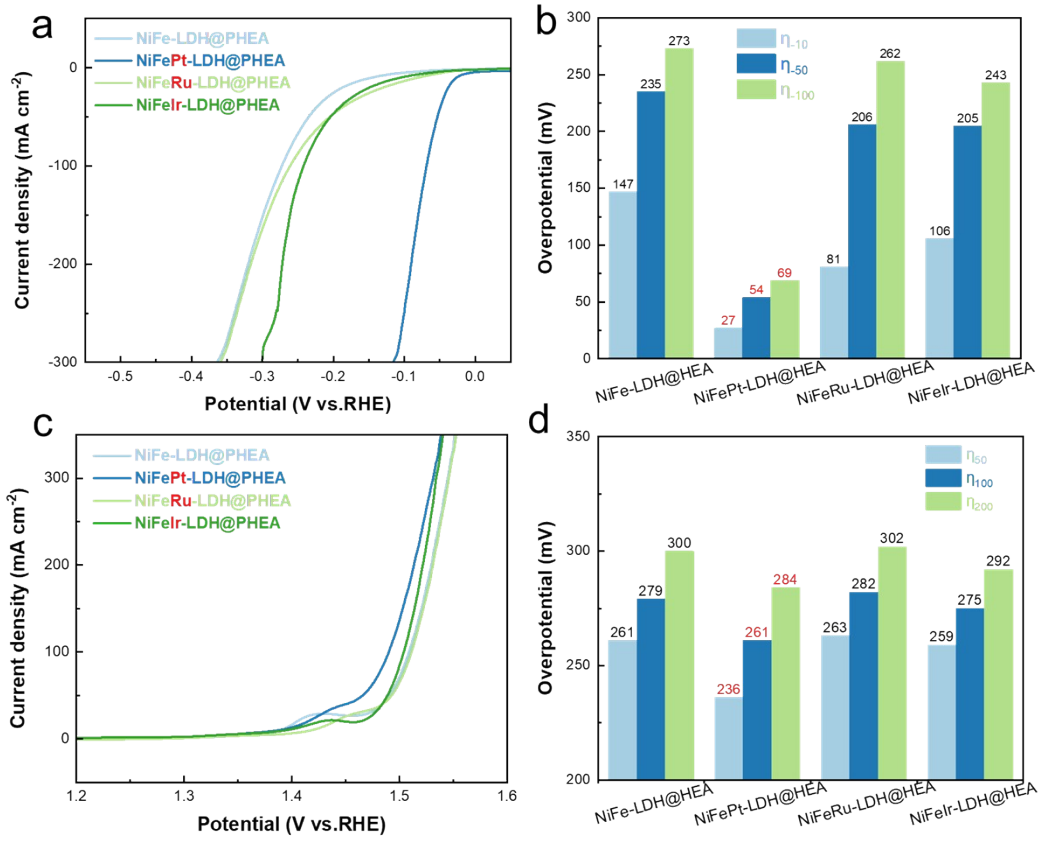

Figure S8. HER and OER performance for NiFeY(Y=Pt, Ru, Ir)-LDH@PHEA electrodes. (a) LSV curves for HER performance of various bulk PHEA electrodes. (b) Overpotential for HER of various bulk PHEA electrodes at different current densities (10, 50, 100 mA cm^{-2}). (c) LSV curves for OER performance of various bulk PHEA electrodes. (d) Overpotential for OER of various bulk PHEA electrodes at different current densities (50, 100, 200 mA cm^{-2}).

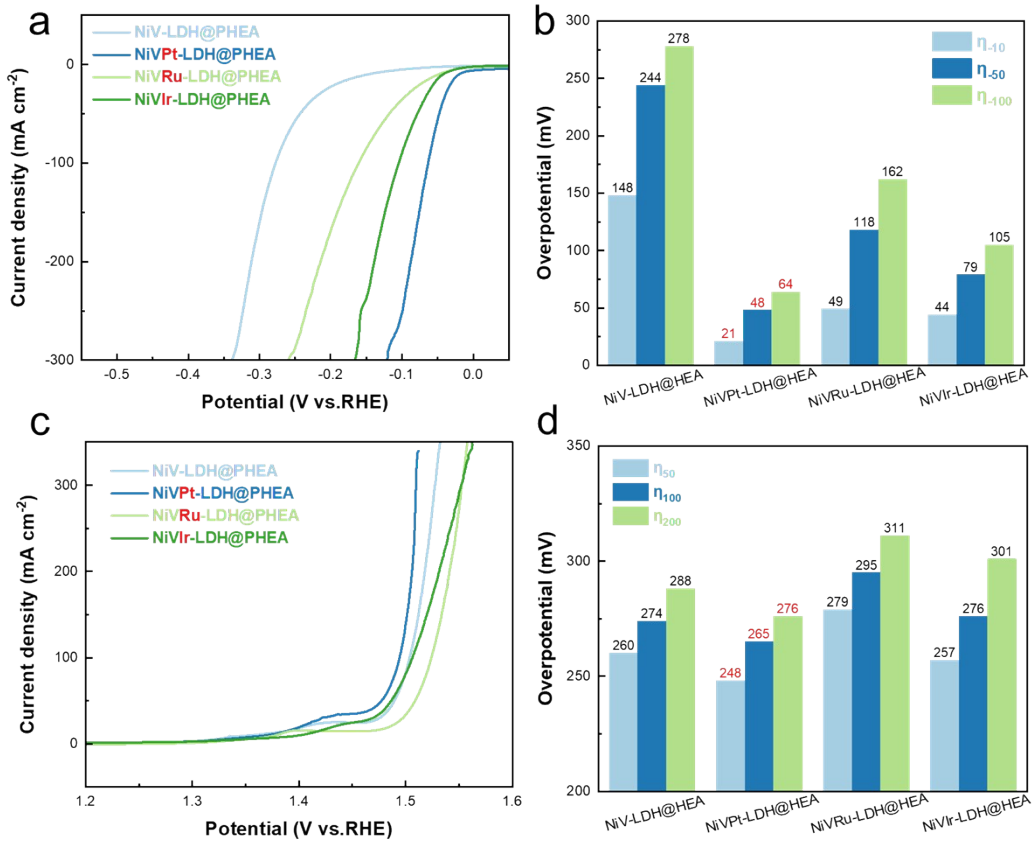

Figure S9. HER and OER performance for NiVY(X=Pt, Ru, Ir)-LDH@PHEA electrodes. (a) LSV curves for HER performance of various bulk PHEA electrodes. (b) Overpotential for HER of various bulk PHEA electrodes at different current densities (10, 50, 100 mA cm^{-2}). (c) LSV curves for OER performance of various bulk PHEA electrodes. (d) Overpotential for OER of various bulk PHEA electrodes at different current densities (50, 100, 200 mA cm^{-2}).

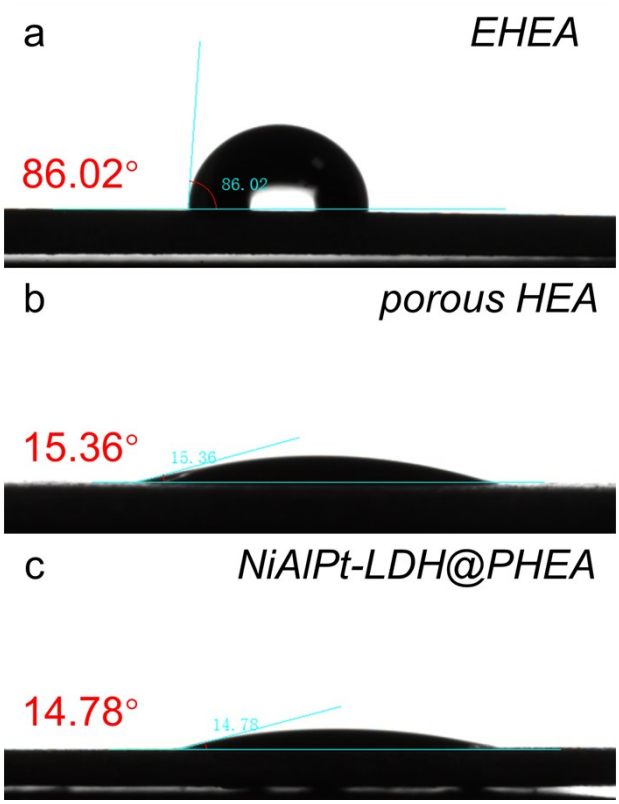

Figure S10. Contact angle test results of various bulk HEA electrodes.

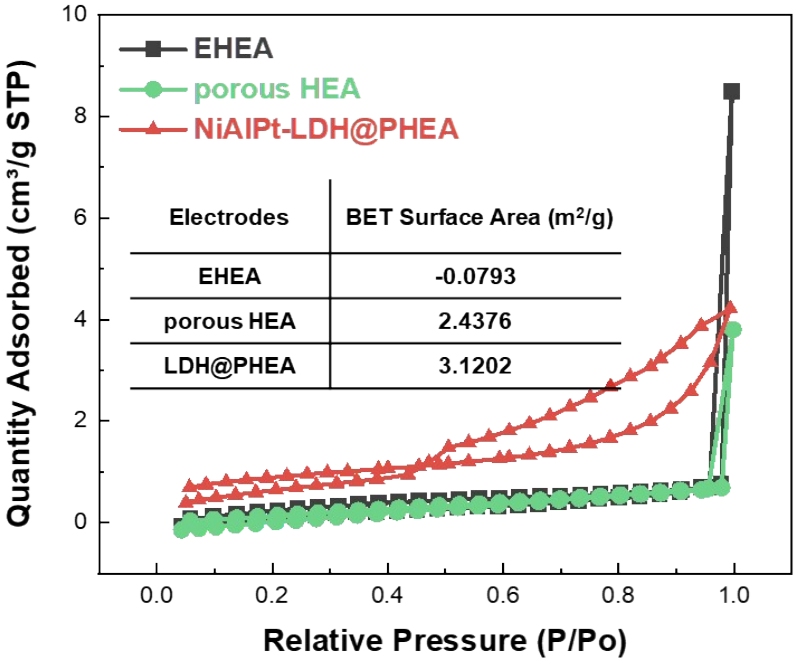

Figure S11. Nitrogen adsorption and desorption curves of various bulk HEA electrodes. The table shows the BET areas.

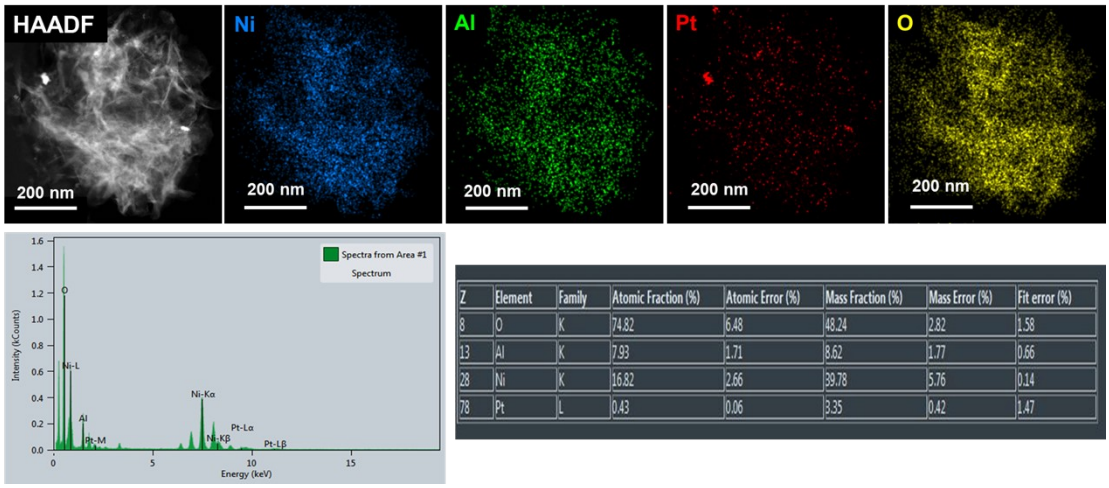

Z	Element	Family	Atomic Fraction (%)	Atomic Error (%)	Mass Fraction (%)	Mass Error (%)	Fit error (%)
8	O	K	74.82	6.48	48.24	2.82	1.58
13	Al	K	7.93	1.71	8.62	1.77	0.66
28	Ni	K	16.82	2.66	39.78	5.76	0.14
78	Pt	L	0.43	0.06	3.35	0.42	1.47

Figure S12.TEM imaging of NiAlPt-LDH including HAADF mapping, element strength diagram and element content table.

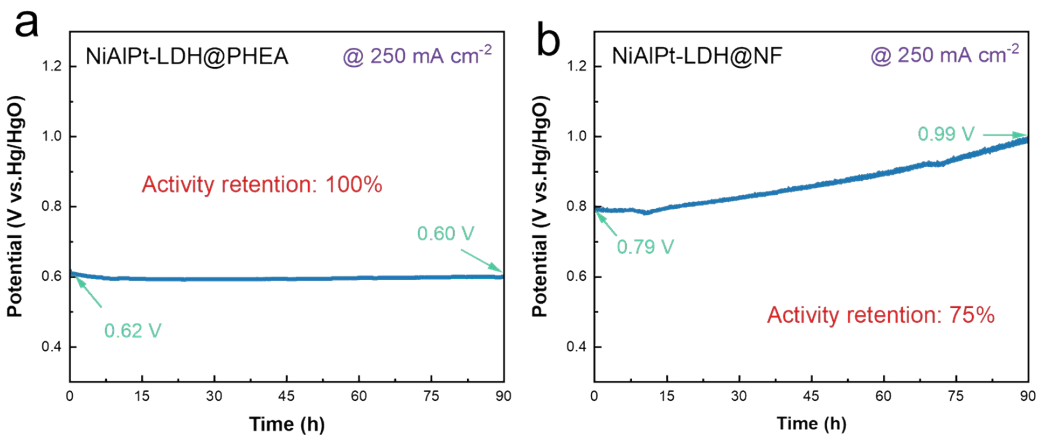

Figure S13. Stability testing of (a) NiAlPt-LDH@PHEA/ (b) NF electrodes at 250 mA cm^{-2} *via* the chronopotentiometry *c-p* technique.

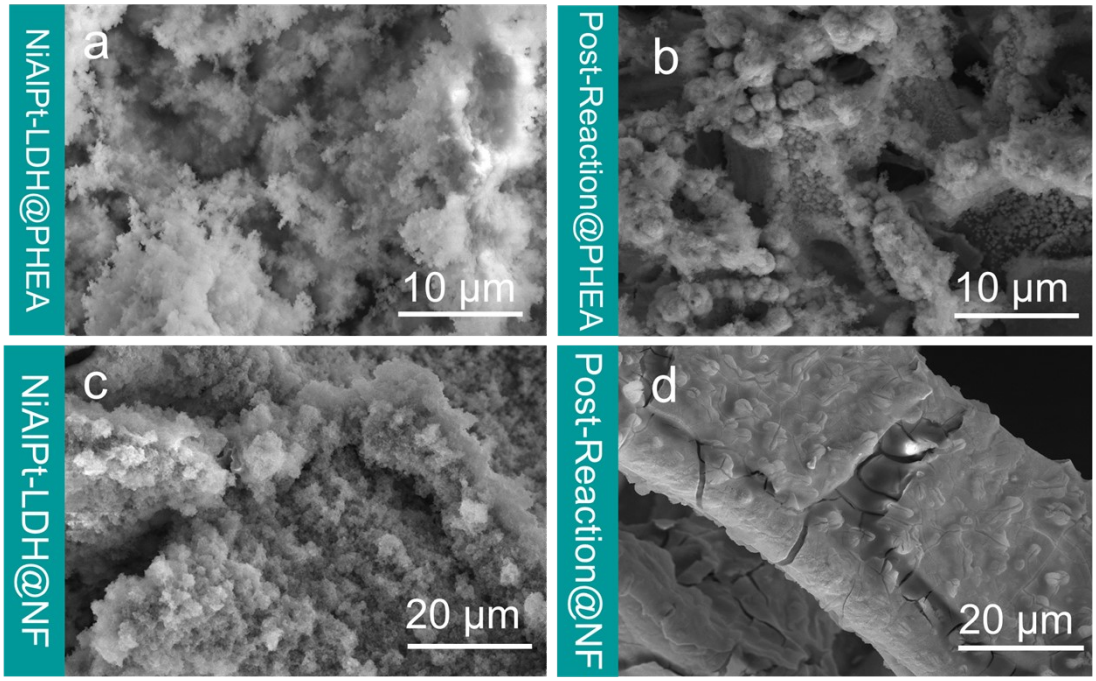

Figure S14.SEM imaging of NiAlPt-LDH@PHEA/NF electrodes before (a, c) and after (b, d) 90 h oxygen evolution reaction.

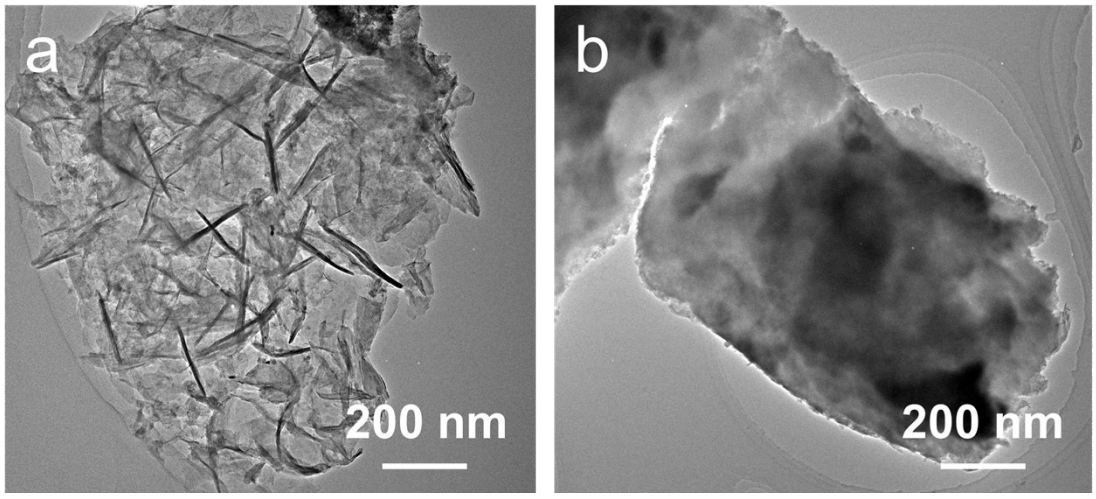

Figure S15. TEM imaging of (a) NiAlPt-LDH@PHEA/ (b) NF electrodes after 90 h oxygen evolution reaction.

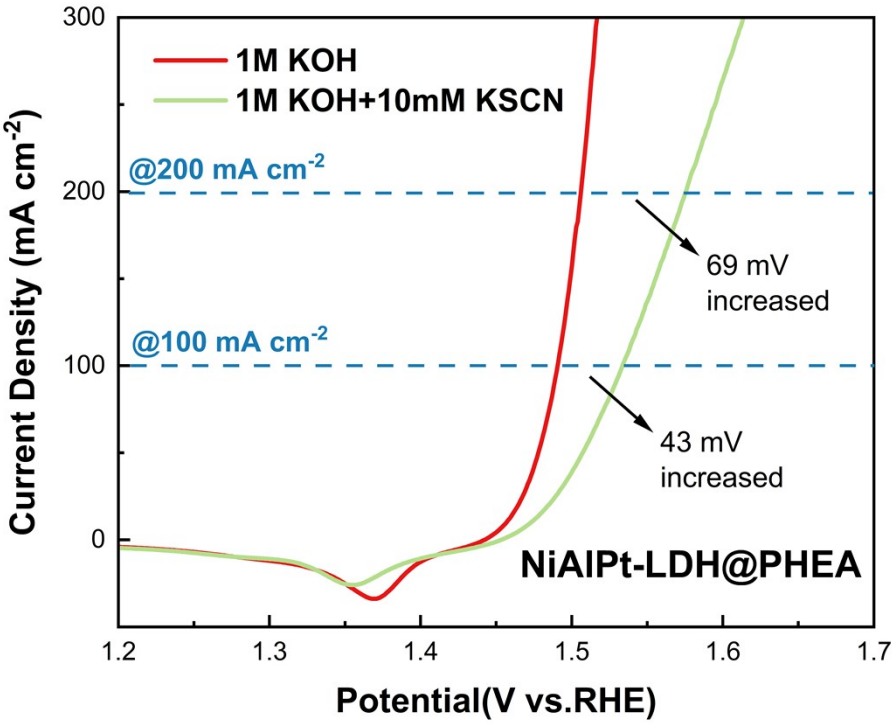

Figure S16. The OER LSV curves of NiAlPt-LDH@PHEA before and after the addition of 10 mM KSCN masking reagent.

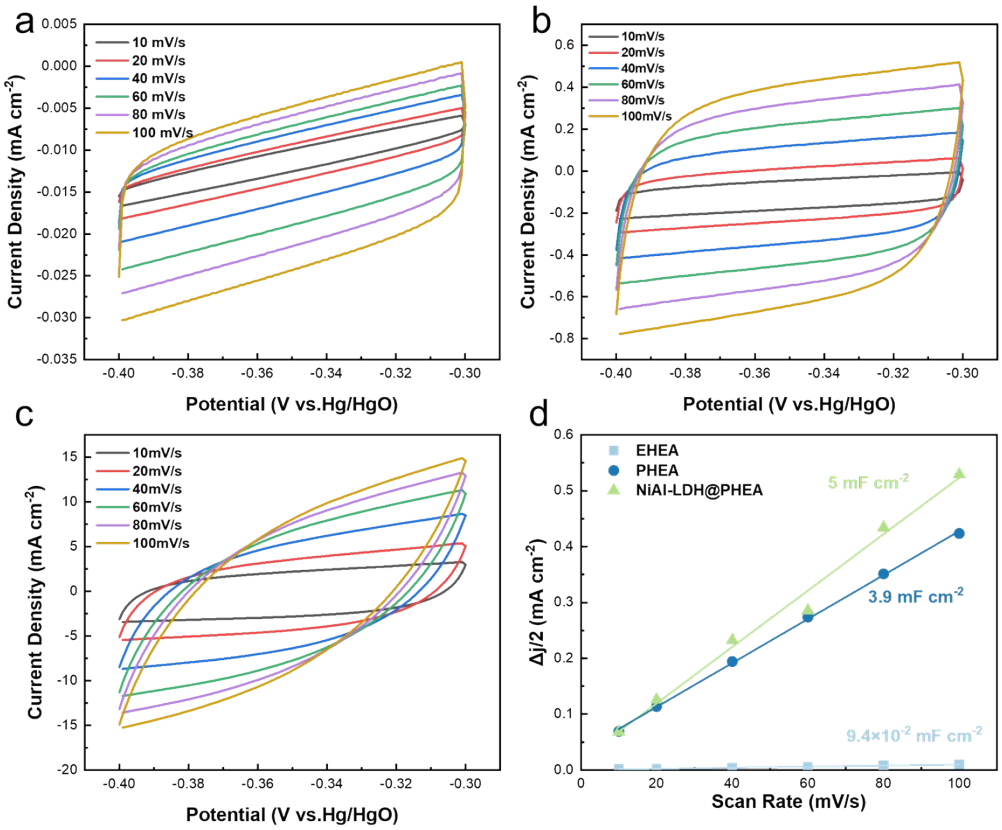

Figure S17. CV curves of various bulk electrodes at different scan rate. (a) EHEA. (b) NiAl-LDH@PHEA. (c) NiAlPt-LDH@PHEA. (d) C_{dl} obtained by CV cycles at given scan rate.

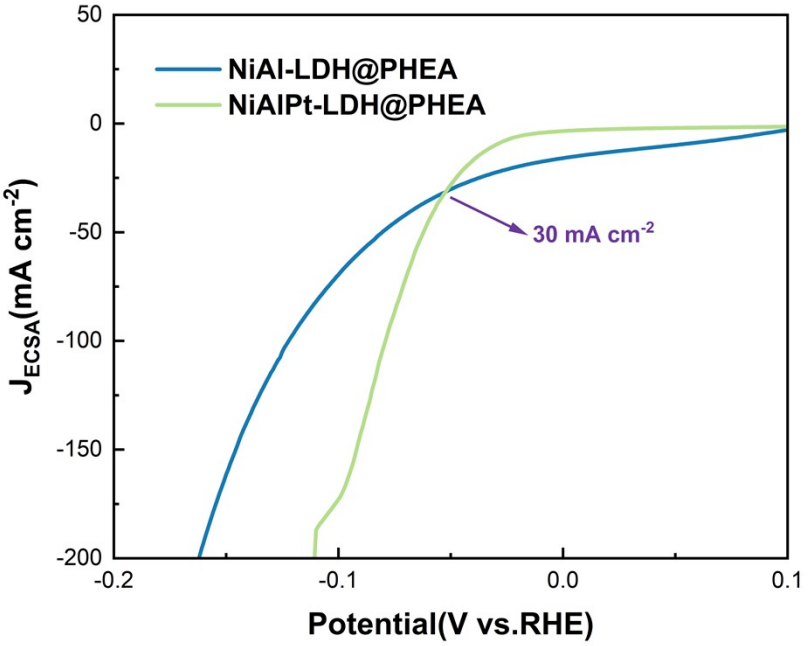

Figure S18. HER activity of various bulk HEA electrodes in 1 M KOH normalized by ECSA.

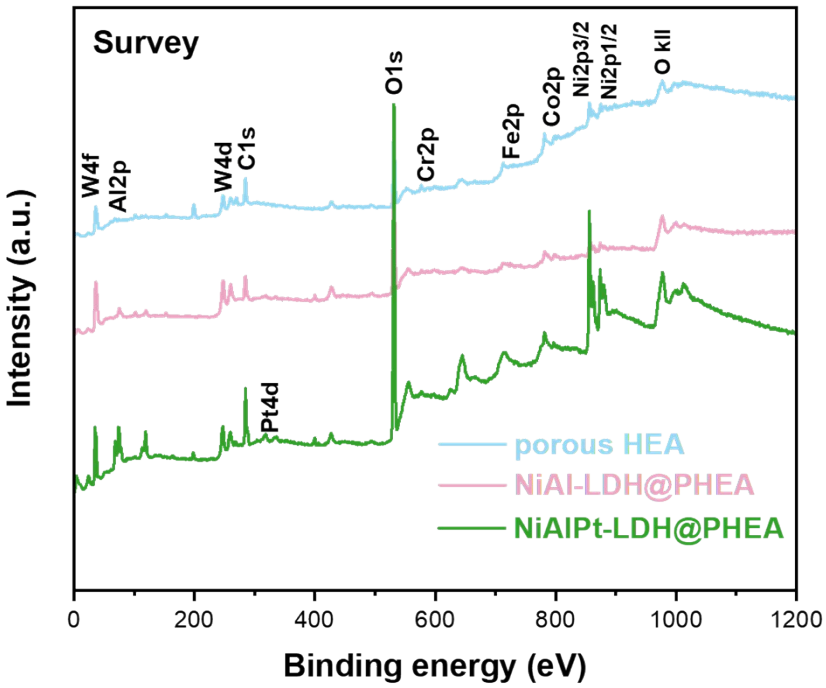

Figure S19. XPS survey spectra of various bulk HEA electrodes.

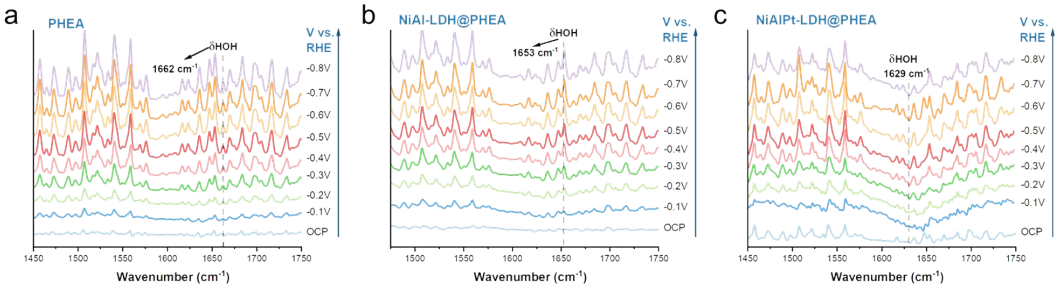

Figure S20. *In situ* electrochemical FT-IR spectra for various bulk HEA electrodes at different potentials. (a) PHEA. (b) NiAl-LDH@PHEA. (c) NiAlPt-LDH@PHEA.

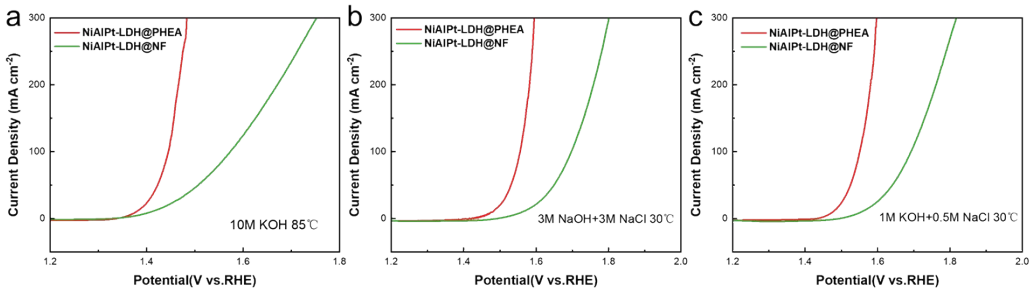

Figure S21. LSV curves for NiAlPt-LDH@PHEA/NF electrodes under different reaction conditions. (a) Industrial electrolytic water. (b) Chlor-alkali Industry. (c) Simulated seawater.

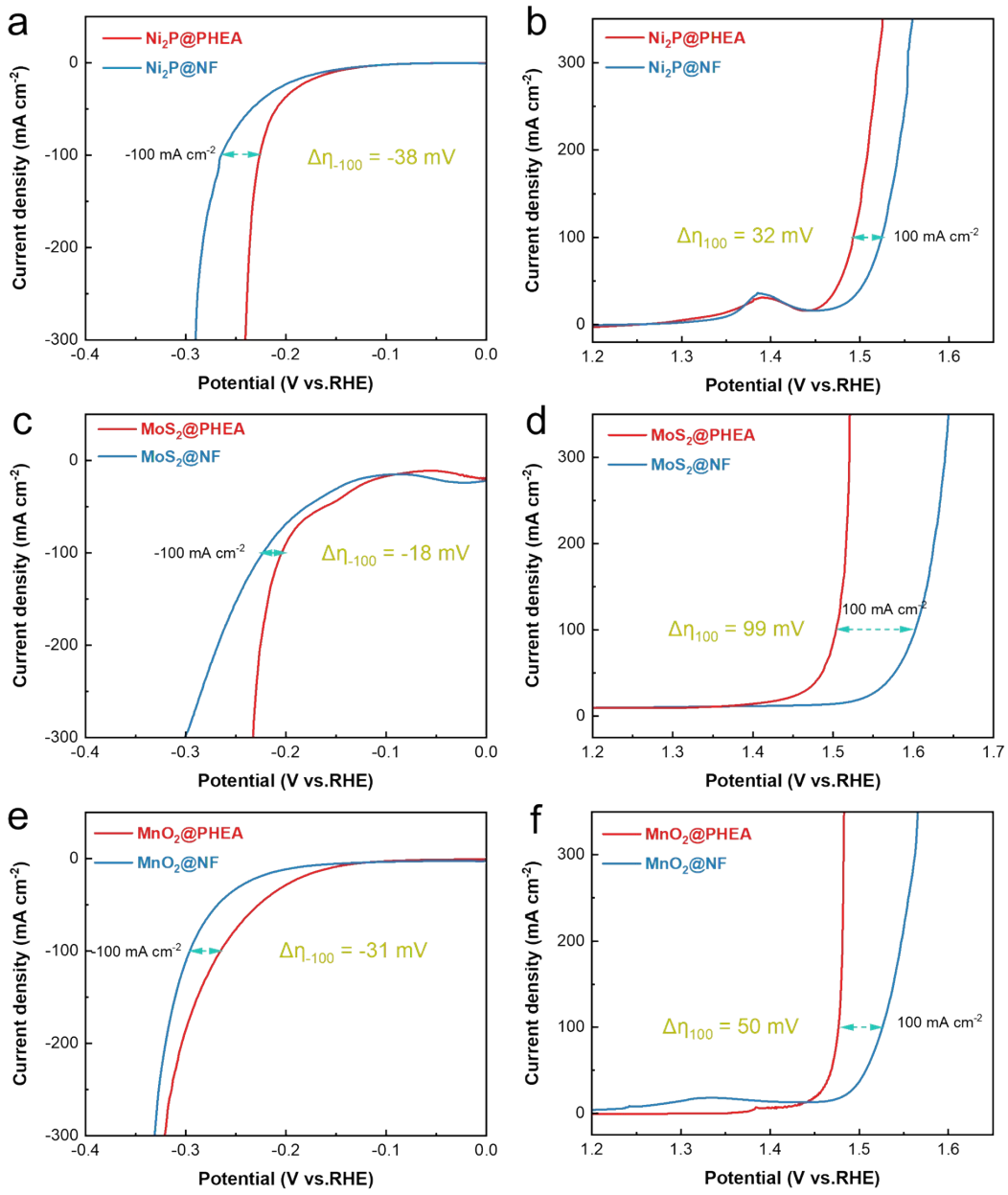

Figure S22. Comparison of HER and OER performance between PHEA and NF substrates modified with different active phases.